Signature of an antiferromagnetic metallic ground state in heavily electron-doped Sr_2FeMoO_6

Somnath Jana,[1] Carlo Meneghini,[2] Prabuddha Sanyal,[3] Soumyajit Sarkar,[3] Tanusri Saha-Dasgupta,[3]
Olof Karis,[4] and Sugata Ray[1,5,*]

[1]*Centre for Advanced Materials, Indian Association for the Cultivation of Science, Jadavpur, Kolkata 700 032, India*
[2]*Dipartimento di Fisica, Universitá di Roma Tre Via della vasca navale, 84 I-00146 Roma, Italy and OGG-GILDA c/o ESRF, Grenoble, France*
[3]*Department of Condensed Matter and Materials Science, S.N. Bose National Centre for Basic Sciences, JD Block, Sector III, Salt Lake, Kolkata 700 098, India*
[4]*Department of Physics and Astronomy, Uppsala University, SE-75121 Uppsala, Sweden*
[5]*Department of Materials Science, Indian Association for the Cultivation of Science, Jadavpur, Kolkata 700 032, India*

(Received 16 February 2012; revised manuscript received 6 June 2012; published 20 August 2012)

Sr_2FeMoO_6 is a well-known double perovskite with exciting high-temperature magnetic properties. Through various magnetic and spectroscopic measurements, we collect compelling evidence here that this compound can be driven into a rare three-dimensional antiferromagnetic metallic state by heavy electron doping (70% Sr^{2+} substitution by La^{3+}). Moreover, local structural study of these $Sr_{2-x}La_xFeMoO_6$ ($1.0 \leqslant x \leqslant 1.5$) compounds reveals unusual atomic scale phase distribution in terms of La,Fe- and Sr,Mo-rich regions driven by strong La-O covalency, a phenomenon hitherto undisclosed in double perovskites. The general trend of our findings is in agreement with theoretical calculations carried out on realistic structures having local chemical fluctuations, which reconfirms the relevance of the kinetic-energy-driven magnetic model.

DOI: 10.1103/PhysRevB.86.054433 PACS number(s): 75.47.Lx, 72.15.Eb, 75.50.Ee, 78.70.Dm

I. INTRODUCTION

A general relationship between electrical conductivity and magnetism is maintained in strongly correlated electron systems in which ferromagnetism accompanies metallic conductivity and antiferromagnetism is associated with insulating behavior. There are only a few examples of antiferromagnetic, metallic (AFM-M) transition-metal oxides, but mostly with layered structures, and only one with a three-dimensional perovskite structure.[1] Therefore, the recent theoretical proposition of realizing a metallic, AFM ground state in La-doped Sr_2FeMoO_6 (SFMO) double perovskites, beyond a critical doping of La,[2,3] sparked curiosity. The theoretical study in terms of *ab initio* calculation as well as the solution of the model Hamiltonian proposed that the stability of this AFM phase arises from the same kinetic-energy-driven mechanism as originally presented[4] for ferromagnetism (FM) in undoped SFMO. According to the theoretical predictions, the AFM-M phase should be observed in $Sr_{2-x}La_xFeMoO_6$ with $x > 1.5$, while there could be a coexistence of FM and AFM phases within a doping range of $1.0 < x < 1.5$. Interestingly, this range of electron doping in SFMO was not explored earlier, although lower doped compounds ($x \leqslant 1.0$) have indeed been investigated before.[5–8] It is, therefore, highly desirable to experimentally probe the large La-doping regime, although it becomes somewhat complicated by the enhanced Fe/Mo site disorder and steric effects with electron doping.[8] Nevertheless, it is worthwhile to explore this untested regime to probe the curious proposal of the existence of an AFM-M phase. Here, we report structural, magnetic, and electronic property studies on $Sr_{2-x}La_xFeMoO_6$ samples (which will be referred to as La_x from now on) with x up to 1.5 (any attempt to go beyond $x = 1.5$ makes the sample impure). Interestingly, the real chemical structure turned out to be dominated by atomic scale phase fluctuation, a very different scenario from the perfect rock-salt ordering or antisite disordered structure commonly encountered in double perovskites, except for the very recent report on $LaSrVMoO_6$.[9,10] Measurements on the series of $Sr_{2-x}La_xFeMoO_6$ samples clearly indicate that the system is on the verge of adopting a metallic, AFM ground state with higher electron doping ($x \geqslant 1.4$). It is also observed that the doped system undergoes magnetic frustration in the whole doping range of $1.0 < x < 1.5$. Consequently, we have also carried out further theoretical calculations, taking into account the realistic chemical structure, that strongly support the experimental observation. Both experimental and theoretical studies reveal that this crossover from ferromagnetic-like to AFM-like behavior is largely dominated by the electronic changes, establishing the importance of the kinetic-energy-driven mechanism[4] once again.

II. EXPERIMENTAL AND THEORETICAL DETAILS

The five different compositions of La_x with $x = 1.0$, 1.1, 1.25, 1.4, and 1.5 were synthesized in polycrystalline form by conventional solid state synthesis. The phase purity of the samples was checked by x-ray diffraction (XRD) using a Bruker AXS: D8 Advance x-ray diffractometer. Magnetic measurements were carried out in a Quantum Design SQUID magnetometer. X-ray absorption spectroscopy (XAS) was carried out in total electron yield mode at the I1011 and D1011 beam lines of the Swedish synchrotron facility MAX-Lab, Lund. The x-ray photoelectron spectroscopic (XPS) measurements were carried out in an Omicron electron spectrometer, equipped with an EA125 analyzer and Mg $K\alpha$ x-ray source with an energy resolution of ~0.5 eV. Both XAS and XPS data were collected after *in situ* surface cleaning using a diamond scraper. Mo K-edge x-ray absorption fine structure (XAFS) measurements were performed at the BM08-GILDA beamline at ESRF (Grenoble).[11] All the XRD, XAS, XPS, and XAFS measurements were performed at room temperature. We also carried out theoretical calculations in order to confirm the experimental observation, both in terms of *ab initio*

density functional theory (DFT) as well as model Hamiltonian approaches, constructed out of DFT calculations.

III. RESULTS AND DISCUSSIONS

Phase analysis from XRD refinement indicated a space group of $P2_1/n$ with small monoclinic distortion for all the compositions. This is in agreement with the literature, in which a transition to monoclinic $P2_1/n$ symmetry from tetragonal $I4/mmm$ symmetry has been reported for a doping level of $x \geqslant 0.4$.[5]

The local chemical structure surrounding Mo ions had been probed by XAFS. Mo K-edge XAFS data were analyzed along the lines already described in Refs. 9,10,12, and 13, with the aim of understanding, at the local scale, the features of Mo-A/A' and Mo-O-B/B' disorder as a function of sample composition. XAFS data and the Fourier transform along with the respective best fit spectra for all the compositions are shown in Figs. 1(a) and 1(b). The data refinement required particular attention to the next-neighbor distribution as the almost collinear Mo-O-B/B' configurations involve non-negligible multiple scattering contributions, which has to be considered with care because they provide details about the local chemical order. The standard XAFS formula[14] is used for data refinement. Theoretical amplitude and phase functions were calculated using the FEFF code[15] in a muffin-tin approximation using Heidin-Lundqvist interatomic potentials. A representative example of XAFS data fitting is shown in Fig. 1(c); the following contributions have been used for all the samples: the MoO, which represents the contribution coming from the six oxygens directly bonded to the Mo absorber, the MoLa and MoSr due to the Mo-A/A' type, and MoOMo and MoOLa coming from the Mo-O-B/B' type connections, each one including single (SS) and multiple scattering (MS) contributions. To keep the number of free parameters in the data refinement reduced, the multiplicity numbers for the different coordination shells are constrained to crystallographic values.

The first shell (MoO) contains six oxygen neighbors around 2.01 Å; this distance increases slightly (up to 2.04 Å) upon raising the La content x. More interesting is the evolution of the Mo-A/A' and Mo-O-B/B' shells. Here, data refinement is achieved fixing the total multiplicity to $N_{\mathrm{Mo}A} = 8$ and $N_{\mathrm{Mo}OB} = 6$, respectively, and refining two parameters: y_A, being the fraction of Mo-Sr neighbors, and y_B, being the fraction of Mo-O-Mo connections. In this way, we obtained the most relevant local structural information from XAFS analysis and the picture of local chemical order around Mo, namely the number of Mo-Sr (Mo-La) neighbors: $N_{\mathrm{Mo}A} \times y_A$ [$N_{\mathrm{Mo}A} \times (1 - y_A)$], and the number of Mo-O-Mo (Mo-O-Fe) connections: $N_{\mathrm{Mo}OB} \times y_B$ [$N_{\mathrm{Mo}OB} \times (1 - y_B)$], which are presented in Table I. Now, in case of a perfectly ordered Fe/Mo arrangement, the number of Mo-O-Mo connections should be 0; for a completely random situation, this number should be 3; and for an $A\mathrm{MoO_3}$-like phase, it should be 6. Interestingly, the XAFS data show, in all the compounds, the Mo-O-Mo connectivity to be larger than 3 (random distribution), indicating the presence of an $A\mathrm{MoO_3}$-like environment. Similarly, for a random distribution of x La and $(2 - x)$ Sr atoms in the lattice, each Mo should be surrounded by $(8 - 4x)$ Sr atoms and $4x$ La atoms, while experimental data reveal that there is a large preferential accumulation of Sr ions around the Mo sites, signaling the formation of Sr,Mo-rich patches. Therefore, XAFS experiments revealed the development of Sr,Mo-rich and consequently La,Fe-rich short-range patches within the

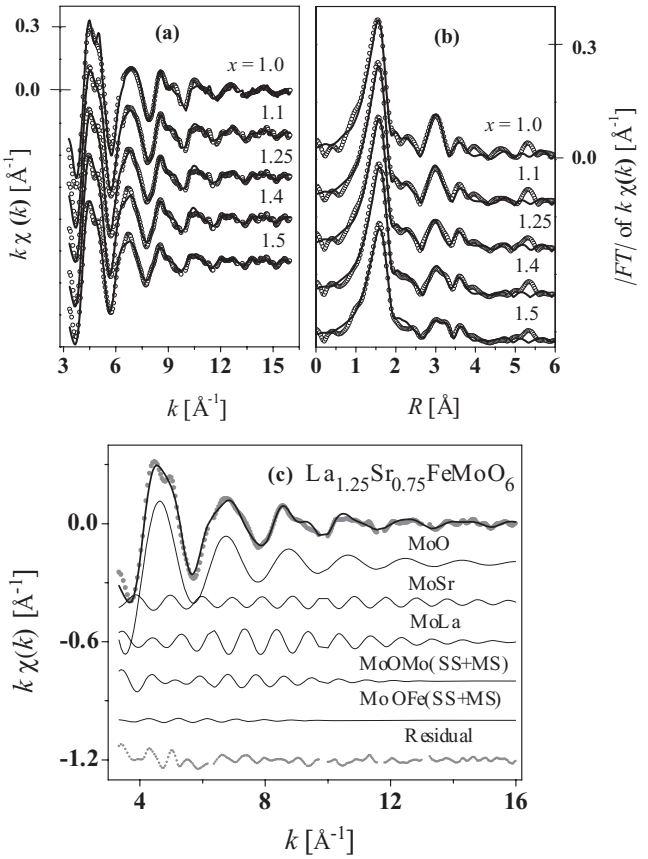

FIG. 1. (a) The k weighted XAFS data (open circles) plotted together with the best fit (black lines). (b) Fourier transform of experimental (open circles) data plotted together with the fitted (dark lines) curves. (c) Representative example of XAFS data fitting for the $La_{1.25}$ sample composition: experimental data $k\chi^{\mathrm{exp}}$ (points) and best fit $k\chi^{\mathrm{theor}}$ (full line) are shown at the top and, shifted for clarity, the partial contributions are reported. The lower curve represents the best fit residual: $k\chi^{\mathrm{exp}} - k\chi^{\mathrm{theor}}$.

TABLE I. Mo-K edge XAFS results. N indicates experimentally observed connectivities, while $(8 - 4x)$ is the ideal Mo-Sr connectivity for a perfect homogeneous distribution of A-site ions. The coordination numbers are constrained to a crystallographic structure. The mismatch between experimental data and the best fit is $R^2 = 0.077$.

	Mo-O-Mo			Mo-Sr		
x	N	R (Å)	σ^2 ($\times 10^2$ Å^2)	$N(8-4x)$	R (Å)	σ^2 ($\times 10^2$ Å^2)
1.0	4.35	3.91	0.70	6.0 (4.0)	3.48	0.72
1.1	4.43	3.92	0.82	6.0 (3.6)	3.48	0.74
1.25	5.18	3.92	1.33	5.8 (3.0)	3.49	0.58
1.4	4.65	3.90	0.86	5.4 (2.4)	3.51	0.55
1.5	4.28	3.90	0.70	4.7 (2.0)	3.53	0.68

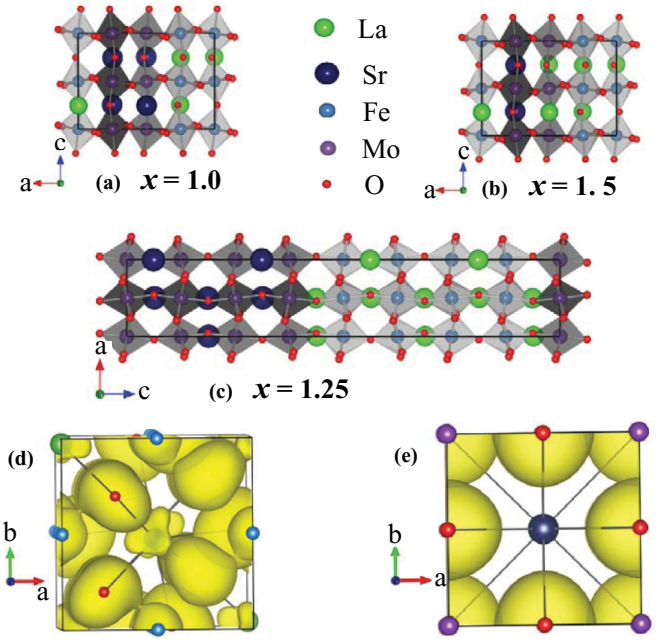

FIG. 2. (Color online) (a)–(c) Representative supercells for $x = 1.0$, 1.5, and 1.25 constructed following the XAFS data. (d) and (e) Charge density plots for $LaFeO_3$ and $SrMoO_3$, respectively.

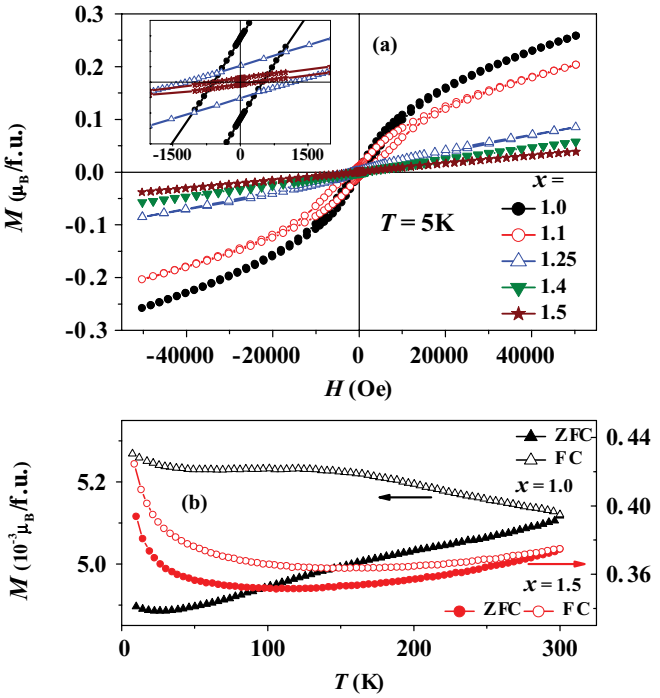

FIG. 3. (Color online) (a) Magnetization plotted as a function of varying field for all the compositions. Inset shows the zoomed view of the plot close to the origin for $x = 1.0$, 1.25, and 1.5. (b) ZFC-FC magnetization data plotted as a function of temperature for $x = 1.0$ and 1.5 samples.

systems, which is very similar to the recent observation in $LaSrVMoO_6$.[9] The smallest unit cells that satisfy the local Mo-Sr and Mo-O-Mo connectivity for $x = 1.0$, 1.5, and 1.25 are shown in Figs. 2(a)–2(c), respectively. It should be noted that these unit cells exhibit only a representative situation capturing the essential, while the actual structure may be more complex. *Ab initio* calculation reveals that the formation of a patchy structure is driven by strong La-O covalency, which competes with the stronger Mo-O covalency compared to the weaker Fe-O covalency,[10] as shown in the calculated charge density plots in Figs. 2(d) and 2(e). As a result, it is energetically favorable for La to be in the surrounding of Fe, which helps to satisfy the covalency between the La and the O, which is connected to two weakly covalent Fe ions.[10] Interestingly, this atomic-scale phase separation further shows a nonmonotonic dependence on x, with a maximum arising around $x = 1.25$ (see Table I). This nonmonotonic behavior can also be rationalized in terms of stronger La-O covalency. For a composition with larger x, it becomes necessary to accommodate Mo ions in the vicinity of the La ions, and within the geometry of a growing patchy structure, a possibility arises that a $LaMoO_3$-like phase will develop, which would be highly unfavorable. Therefore, it becomes preferable for the system to adopt a more homogeneous ionic distribution so that most of the La finds at least some Fe ions around it.

The magnetization (M) versus field (H) data at 5 K [see Fig. 3(a)] show that the magnetic moment at higher fields (5 T) is significantly less compared to what is expected from a perfectly ordered, ferrimagnetic sample. This behavior is consistent with the literature, at least for the $La_{1.0}$ sample,[5,16,17] and is generally explained by an enhanced contribution from superexchange driven Fe-O-Fe AFM interaction, resulting from increased antisite disorder with doping.[18,19] However, the trend of the $M(H)$ curves indicates a sharp change after $x = 1.1$ and the $M(H)$ curve already becomes nearly linear for $x = 1.25$, although a finite hysteresis persists (see the inset). The magnetic coercivity gradually decreases with increasing x, and the $M(H)$ from the $La_{1.5}$ sample closely resembles an antiferromagnetic $M(H)$ curve. Out of five samples, two sets of ZFC-FC $M(T)$ data from the two end compositions measured at a field of 200 Oe are presented in Fig. 3(b). All the ZFC-FC curves exhibit divergences, indicating magnetic metastability, presumably originating from the coexistence of FM and AFM interactions, but there is a gradual reduction in susceptibility as well as in the bifurcation between the ZFC and FC curves with increasing x, which indicates a steady crossover toward an antiferromagnetic-like ground state. It should be noted that the growth of the AFM-like magnetic state is not proportional to the available Fe-O-Fe AFM connections, which in fact decreases for compositions with $x > 1.25$. This establishes that the observed crossover in magnetic behavior is *entirely* guided by changes in the electronic structure as a result of gain in kinetic energy,[3] and is uncorrelated to Fe-O-Fe superexchange, effective in the Fe-rich regions.

To corroborate the experimental results and also to check the validity of the previous prediction[3] of an AFM-M phase in La-doped SFMO, which did not consider the experimentally observed patchy structures, we carried out further theoretical calculations. Evidently, several possible supercells with patchy structures could be constructed with varying distributions of La, Fe-rich and Sr, Mo-rich regions, which would be consistent with the XAFS findings. Unfortunately, it becomes computationally prohibitive to carry out first-principles calculations even for the simplest supercells [shown in Figs. 2(a)–2(c)],

while in reality it is expected that the composition fluctuation would be much more random than what is accommodated in these supercells. To overcome this difficulty, we resort to the model Hamiltonian approach, and we introduced the following low-energy, multiorbital model Hamiltonian, the parameters of which were obtained from *ab initio* calculations:

$$\begin{aligned} H = {} & \epsilon_{\mathrm{Fe}} \sum_{i\in B} f^{\dagger}_{i\sigma\alpha} f_{i\sigma\alpha} + \epsilon_{\mathrm{Mo}} \sum_{i\in B'} m^{\dagger}_{i\sigma\alpha} m_{i\sigma\alpha} \\ & - t_{\mathrm{FM}} \sum_{\langle ij\rangle\sigma,\alpha} f^{\dagger}_{i\sigma\alpha} m_{j\sigma\alpha} - t_{\mathrm{MM}} \sum_{\langle\langle ij\rangle\rangle\sigma,\alpha} m^{\dagger}_{i\sigma\alpha} m_{j\sigma\alpha} \\ & - t_{\mathrm{FF}} \sum_{\langle\langle ij\rangle\rangle\sigma,\alpha} f^{\dagger}_{i\sigma\alpha} f_{j\sigma\alpha} + J \sum_{i\in A} \mathbf{S}_i \cdot f^{\dagger}_{i\alpha} \vec{\sigma}_{\alpha\beta} f_{i\beta} \\ & + J_{\mathrm{AS}} \sum_{\langle\langle ij\rangle\rangle} \mathbf{S}_i \cdot \mathbf{S}_j, \end{aligned}$$

where f's (m's) refer to the Fe (Mo) sites. t_{FM}, t_{MM}, and t_{FF} represent the nearest-neighbor Fe-Mo, Mo-Mo, and Fe-Fe hoppings, which happen at the interface of the patches and within the Mo-rich and Fe-rich patches, respectively. σ is the spin index and α is the orbital index that spans the t_{2g} manifold of the Fe and Mo d orbitals. The $\mathbf{S}_i$'s are "classical" core spins at the Fe site, coupled to the itinerant electrons at the Mo site through J.[4] The parameter J_{AS} controls the superexchange driven coupling between Fe spins in Fe-rich patches. The parameters of the model Hamiltonian were extracted[20] from the first-principles calculations through Nth-order muffin-tin orbital (NMTO)-based downfolding calculations,[21] as has been explained in Ref. 2. This model was then solved using exact diagonalization on a patchy supercell, closer to the real structure. The total energies calculated considering the FM as well as AFM alignment of Fe spins are plotted in Fig. 4. Evidently, even in the presence of a patchy structure, the AFM solution takes over the FM solution beyond a critical value of the number of valence electrons, which translates to the critical concentration of La. We find that the crossover happens around a concentration of $x = 1.0$, with a small energy difference between the two solutions (of the order of a few meV), thus there is the possibility of phase coexistence around the crossover point, which is what is recognized experimentally. Also, it is interesting to note that even the current theoretical calculations predict metallic behavior for the AFM state, as stabilization of the AFM state is hopping-driven. To experimentally confirm this, we then carried out XPS valence-band experiments on all the samples.

Area normalized (between −2 and 14 eV) valence band spectra from the five samples are summarized in Fig. 5. The first important observation is the presence of clear Fermi cutoffs in all the samples, confirming metallicity in all, including the $x = 1.5$ sample. It is also important to note that the intensity of the feature just below Fermi energy, constituted by hybridized Fe t_{2g}, Mo t_{2g}, and O p bands for the ferromagnetic case, exhibits a nonmonotonic behavior with doping. This intensity increases strongly by going from $x = 1.0$ to 1.1, which is expected for electron doping in the ferromagnetic system.[3] It has been clearly shown in theory that there would be a sudden enhancement in DOS for a La concentration approaching the FM-AFM transition because the Fermi energy enters a crest (see Figs. 3 and 5 of Ref. 3),

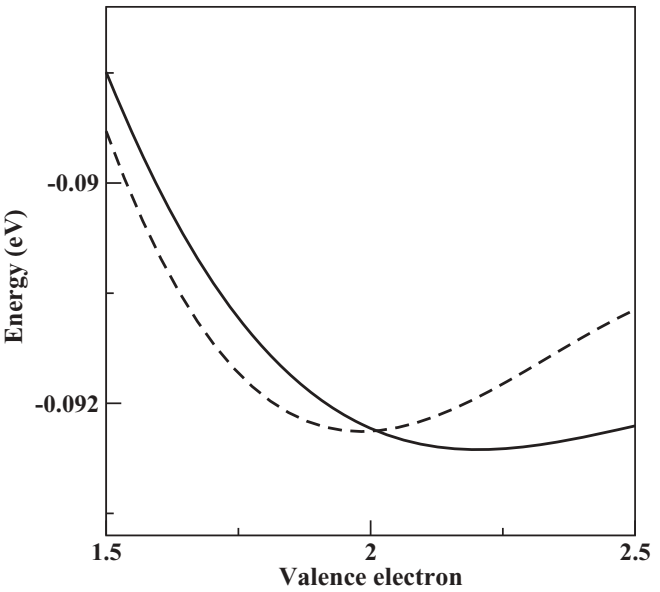

FIG. 4. Total energies for ferromagnetic (dashed line) and antiferromagnetic alignment of Fe spins, plotted as a function of the number of valence electrons, as obtained by exact diagonalization of the low-energy Hamiltonian for a 16 × 4 × 4 lattice with a patchy structure. The number of valence electrons (n) is related to La doping (x), as $n = 1 + x$, as pure Sr_2FeMoO_6 contains one valence electron.

while the DOS dips immediately after the transition (see Figs. 4 and 5 of Ref. 3). In accordance with the theory, the intensity starts to deplete for $x > 1.1$ with AFM behavior gradually taking over as a result of further increase in x (see Fig. 4). Finally, a sharp reduction is observed in the case of $x = 1.5$, which is also consistent with the theoretical prediction of a trough in the AFM DOS at large doping.[3] It is worth mentioning here that different protocols for normalization of the valence band spectra always revealed the same trend. This, in turn, strengthens our proposed scenario, which is robust against different normalization procedures. Also, this set of valence band spectra shows a marked decrease in intensity at around 8 eV binding energy. In the case of SFMO, this valence band feature has been shown to be a Coulomb correlation driven satellite feature, possessing substantial Fe 3d and Mo 4d contributions,[22] where the Mo contribution comes mainly

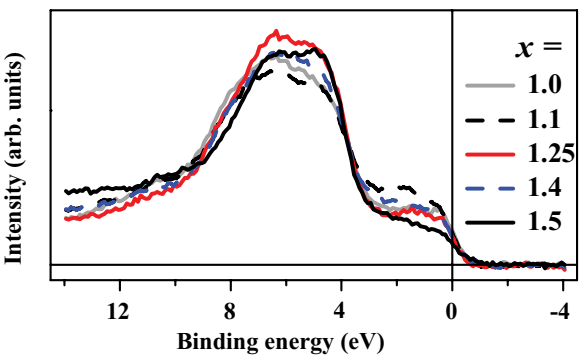

FIG. 5. (Color online) Valence band spectra from all the compositions at 300 K.

through the strong Fe-Mo hybridization as described in the kinetic-energy-driven ferromagnetic mechanism.[4] However, for an AFM ground state, the Mo contribution gets strongly depressed, as has been theoretically shown in the case of La_2FeMoO_6 while going from a FM to an AFM-A magnetic structure.[3] Therefore, the strong reduction of intensity at around 8 eV binding energy of the valence band only endorses the fact that the AFM interaction becomes dominant for the $x = 1.5$ system.

According to the theoretical understanding, the doped electrons exclusively go to the Mo site, and after a certain doping level above $2.0e$/f.u. ($x > 1.0$), the FM state becomes unstable and an AFM state takes over. To address the doping trend, we have performed Fe L-edge XAS and Mo $3d$ core level XPS. In the main panel of Fig. 6(a), all the Fe XAS spectra are plotted. The left inset presents an expanded view of the $2p_{3/2}$ peak, which closely follows the spectral variation with doping. A regular reduction of the higher energy peak up to $x = 1.4$, followed by a sudden flip of the trend at $x = 1.5$, could be observed very clearly. This observation indicates a gradual increase of electron population in the Fe band (Fe^{3+} to Fe^{2+} changeover) up to $x = 1.4$ and a sharp decrease at $x = 1.5$. It should be noted that this observation has been reproduced under proper *in-situ* cleaning and on different batches of samples. We have fitted the experimental Fe XAS spectra as a linear combination of standard Fe^{2+} and Fe^{3+} spectra, acquired from standard literature.[23] The right inset of Fig. 6(a) shows a representative set of observed (open circle) and fitted curves (solid line) together with the related spectral weight corresponding to Fe^{2+} (dashed) and Fe^{3+} (dashed-dot) standard spectra for the $La_{1.25}$ sample. The change of charge on the Fe site in all the samples with respect to $La_{1.0}$, obtained from this fitting, has been shown in Fig. 6(c).

In the main panel of Fig. 6(b), Mo $3d$ core level XPS spectra are plotted for the whole composition range. Although a monotonic intensity enhancement at lower binding energy as a function of increased electron doping is very clear from the plot, the enhancement is much more prominent for the $x = 1.5$ sample. We have fitted all the data by a linear combination of a few spin-orbit-split Mo $3d$ doublets, and a reasonable fitting could be carried out only after considering four such Mo signals, separated by ~1.2 eV from each other, and each having a spin-orbit splitting of ~3.2 eV. The inset of Fig. 6(b) shows the observed (open circle), fitted (solid), and difference (dash) curves together with the corresponding four doublets for the $x = 1.25$ sample. It is rather puzzling to note that the strongest Mo signal comes at a binding energy corresponding to a Mo^{6+} species, which is inconceivable for these compounds. However, this has been a consistent observation for any Mo-based double perovskites, including the parent SFMO (whose nominal constituent is Mo^{5+}),[4,24] or even $LaSrVMoO_6$ (whose nominal constituent is Mo^{4+}).[10] Therefore, for a long time this was a matter of argument until Jaili *et al.*[24] convincingly showed that the intensity of these spurious Mo^{6+} peaks decreases continuously and finally becomes largely suppressed when Sr_2FeMoO_6 film surfaces are *in-situ* sputtered for a prolonged time. Following these experimental results, it was concluded that the formation of oxidized $SrMoO_4$-like phase(s) occurs readily on the surface of such molybdates upon

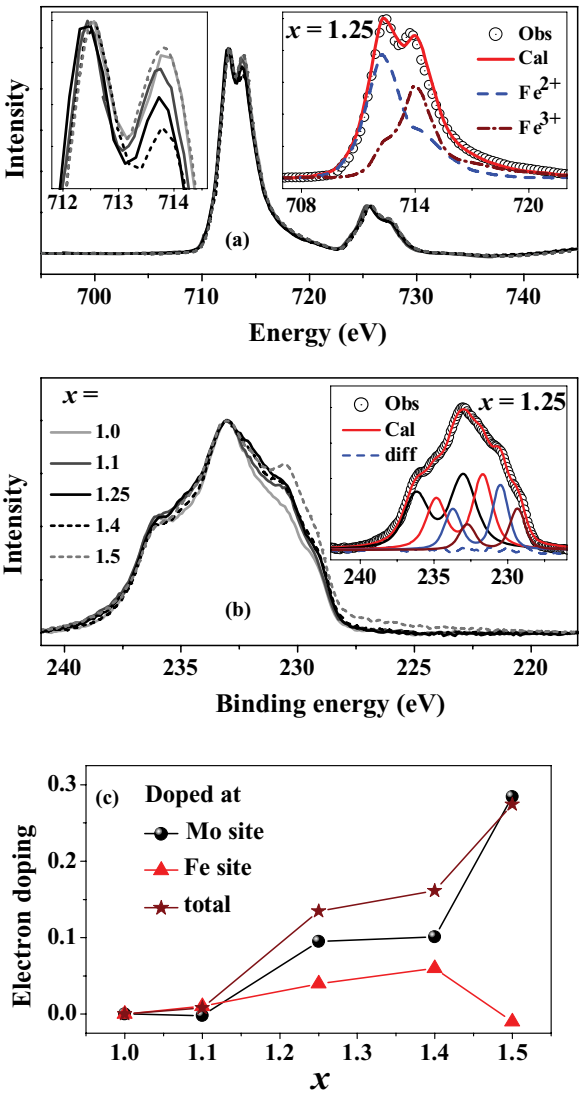

FIG. 6. (Color online) (a) Fe L-edge XAS are plotted for all the compositions. Left inset shows the zoomed portion of the $2p_{3/2}$ and the right inset is the observed and fitted data for the $x = 1.25$ composition. (b) Mo $3d$ core level spectra are plotted for all the compositions. Inset shows the representative fitting corresponding to the $x = 1.25$ composition. (c) Experimental electron doping at the Mo, Fe sites as a function of x.

exposure to air. Therefore, in the present case, it was assumed that the observed Mo^{6+}-like doublet in the XPS experiment, which is known to be a highly surface-sensitive technique,[25] originates from the oxidized surface and has no relationship with the intrinsic electronic structure of the material. Thus, we have calculated the Mo valence excluding the doublet corresponding to the 6+ state, and rather normalized all the spectra with respect to this extrinsic part of the signal, which is expected to remain almost the same for all the samples under identical experimental conditions. The calculated charge at the Mo site for all the samples relative to $La_{1.0}$ is plotted in Fig. 6(c).

Figure 6(c) shows the experimentally obtained variations in Fe, Mo, and total charges with doping. It is interesting to note that up to $x = 1.4$, the doped electrons populate both Fe

and Mo bands, but at $x = 1.5$, almost all the doped electrons shift solely to the Mo site, as was predicted in the theoretical calculation for ordered double-perovskite structure.[3] It can be qualitatively argued that in the observed patchy structure, La is preferably placed within the cage of Fe-O-Fe and this proximity of La and Fe presumably hinders the transfer of the doped electrons to the distant Mo site. As the proportion of Fe-O-Mo connectivity increases at $x = 1.5$, all the doped electrons get transferred to the Mo site.

IV. CONCLUSION

The electronic and magnetic structures of $Sr_{2-x}La_xFeMoO_6$ double perovskites with $x \geqslant 1.0$ have been studied in detail, for which an unusual AFM-M state was predicted. XAFS analysis indicates that all the samples contain small La,Fe-rich and Sr,Mo-rich patches, originating from strong La-O covalency. Detailed magnetic measurements provide an indication of a crossover from a dominant ferromagnetic to a dominant antiferromagnetic state upon increasing La doping. The XPS valence band shows metallic behavior for all the compounds, while indication of an AFM ground state is also revealed at least for the $x = 1.5$ compound. The theoretical calculations, after considering La,Fe- and Sr,Mo-rich short-range patches, confirm that the stability of the AFM-M phase persists even in the presence of local chemical fluctuation. Interestingly enough, our combined experimental and theoretical studies point to the role of a kinetic-energy-driven mechanism in the enhanced stabilization of the AFM state in the large doping regime. Our study, therefore, may prompt experimental research along similar lines for other classes of double perovskites, such as Cr-based $3d$-$5d$ compounds,[26] as well as other systems such as pyrochlores[27] and dilute magnetic semiconductors,[28] for which similar a kinetic-energy-driven mechanism has also been proposed.

ACKNOWLEDGMENTS

S.J. and S.S. thank CSIR, India for financial support. S.R. thanks DST Fast Track, India for financial support. The work was supported by the Swedish Foundation for International Cooperation in Research and Higher Education. We also thank S. Acharya and D. D. Sarma and their DST SR/S5/NM-47/2005 project for making the photoemission studies possible.

*mssr@iacs.res.in

[1] A. C. Komarek, S. V. Streltsov, M. Isobe, T. Möller, M. Hoelzel, A. Senyshyn, D. Trots, M. T. Fernández-Díaz, T. Hansen, H. Gotou, T. Yagi, Y. Ueda, V. I. Anisimov, M. Grüninger, D. I. Khomskii, and M. Braden, Phys. Rev. Lett. **101**, 167204 (2008).

[2] P. Sanyal and P. Majumdar, Phys. Rev. B **80**, 054411 (2009).

[3] P. Sanyal, H. Das, and T. Saha-Dasgupta, Phys. Rev. B **80**, 224412 (2009).

[4] D. D. Sarma, P. Mahadevan, T. Saha-Dasgupta, S. Ray, and A. Kumar, Phys. Rev. Lett. **85**, 2549 (2000).

[5] D. Sánchez, J. A. Alonso, M. García-Hernández, M. J. Martínez-Lope, M. T. Casais, and J. L. Martínez, J. Mater. Chem. **13**, 1771 (2003).

[6] T. Alamelu, U. V. Varadaraju, M. Venkatesan, A. P. Douvalis, and J. M. D. Coey, J. Appl. Phys. **91**, 8909 (2002).

[7] L. Pinsard-Gaudart, R. Surynarayanan, A. Revcolevschi, J. Rodriguez-Carvajal, J.-M. Greneche, P. A. I. Smith, R. M. Thomas, R. P. Borges, and J. M. D. Coey, J. Appl. Phys. **87**, 7118 (2000).

[8] J. Navarro, J. Nogués, J. S. Munõz, and J. Fontcuberta, Phys. Rev. B **67**, 174416 (2003).

[9] S. Jana, V. Singh, S. D. Kaushik, C. Meneghini, P. Pal, R. Knut, O. Karis, I. Dasgupta, V. Siruguri, and S. Ray, Phys. Rev. B **82**, 180407(R) (2010).

[10] S. Jana, V. Singh, A. Nag, C. Meneghini, I. Dasgupta, G. Aquilanti, and S. Ray, Phys. Rev. B **86**, 014203 (2012).

[11] S. Pascarelli, F. Boscherini, F. D'Acapito, J. Hrdy, C. Meneghini, and S. Mobilio, J. Synch. Rad. **3**, 147 (1996).

[12] C. Meneghini, S. Ray, F. Liscio, F. Bardelli, S. Mobilio, and D. D. Sarma, Phys. Rev. Lett. **103**, 046403 (2009).

[13] C. Menehgini, F. Bardelli, and S. Mobilio, Nucl. Instrum. Methods B **285**, 153 (2012).

[14] P. A. Lee, P. H. Citrin, P. Eisenbergher, and B. M. Kincaid, Rev. Mod. Phys. **53**, 769 (1981).

[15] A. L. Ankudinov, B. Ravel, J. J. Rehr, and S. D. Conradson, Phys. Rev. B **58**, 7565 (1998).

[16] G. Narsinga Rao, S. Roya, C.-Y. Mou, and J. W. Chena, J. Magn. Magn. Mater. **299**, 348 (2006).

[17] A. Kahoul, A. Azizi, S. Colis, D. Stoeffler, R. Moubah, G. Schmerber, C. Leuvrey, and A. Dinia, J. Appl. Phys. **104**, 123903 (2008).

[18] E. K. Hemery, G. V. M. Williams, and H. J. Trodahl, Phys. Rev. B **74**, 054423 (2006).

[19] A. Poddar, R. N. Bhowmik, and I. Panneer Muthuselvam, J. Appl. Phys. **108**, 103908 (2010).

[20] The values for t_{FM}, t_{MM}, t_{FF}, $\epsilon_{Fe} - \epsilon_{Mo}$, and J were found to be -0.26, -0.15, -0.40, -0.5, and 1 eV, respectively, while J_{AS} was chosen to be 5 meV, considering the Néel temperature of $LaFeO_3$.

[21] O. K. Andersen and T. Saha-Dasgupta, Phys. Rev. B **62**, R16219 (2000).

[22] S. Ray, P. Mahadevan, A. Kumar, D. D. Sarma, R. Cimino, M. Pedio, L. Ferrari, and A. Pesci, Phys. Rev. B **67**, 085109 (2003).

[23] P. A. van Aken, B. Liebscher, and V. J. Styrsa, Phys. Chem. Miner. **25**, 323 (1998).

[24] H. Jalili, M. F. Heinig, and K. T. Leung, Phys. Rev. B **79**, 174427 (2009).

[25] J. Navarro, J. Fontcuberta, M. Izquierdo, J. Avila, and M. C. Asensio, Phys. Rev. B **70**, 054423 (2004).

[26] H. Das, P. Sanyal, T. Saha-Dasgupta, and D. D. Sarma, Phys. Rev. B **83**, 104418 (2011).

[27] T. Saha-Dasgupta, M. De Raychaudhury, and D. D. Sarma, Phys. Rev. B **76**, 054441 (2007).

[28] P. Mahadevan, A. Zunger, and D. D. Sarma, Phys. Rev. Lett. **93**, 177201 (2004).